Statistical Properties of Molecular Ions in the Ring Current Observed by the Arase (ERG) Satellite

doi: https://doi.org/10.1029/2019GL084163

Geophysical Research Letters

RESEARCH LETTER
10.1029/2019GL084163

Statistical Properties of Molecular Ions in the Ring Current Observed by the Arase (ERG) Satellite

K. Seki[1], K. Keika[1], S. Kasahara[1], S. Yokota[2], T. Hori[3], K. Asamura[4], N. Higashio[1], M. Takada[1], Y. Ogawa[5], A. Matsuoka[4], M. Teramoto[6], Y. Miyoshi[3], and I. Shinohara[4]

[1]Department of Earth and Planetary Science, Graduate School of Science, University of Tokyo, Tokyo, Japan, [2]Graduate School of Science, Osaka University, Osaka, Japan, [3]Institute for Space-Earth Environmental Research, Nagoya University, Nagoya, Japan, [4]Institute for Space and Astronautical Sciences, JAXA, Tokyo, Japan, [5]National Institute of Polar Research, Tachikawa, Japan, [6]Graduate School of Engineering, Kyushu Institute of Technology, Kitakyushu, Japan

Key Points:
- Frequent TOF-mode ion composition measurements by Arase revealed statistical properties of molecular ions in the ring current
- The molecular ($O_2^+/NO^+/N_2^+$) ions are commonly observed during geomagnetically active periods even during small magnetic storms
- The results suggest that the rapid ion outflow from the deep ionosphere occurs frequently during active periods

Correspondence to:
K. Seki,
k.seki@eps.s.u-tokyo.ac.jp

Citation:
Seki, K., Keika, K., Kasahara, S., Yokota, S., Hori, T., Asamura, K., et al. (2019). Statistical properties of molecular ions in the ring current observed by the Arase (ERG) satellite. *Geophysical Research Letters*, *46*, 8643–8651. https://doi.org/10.1029/2019GL084163

Received 18 JUN 2019
Accepted 17 JUL 2019
Accepted article online 22 JUL 2019
Published online 9 AUG 2019

Abstract Molecular ions in the magnetosphere can be a tracer of fast ion outflows from the deep ionosphere. Statistical properties of molecular ions ($O_2^+/NO^+/N_2^+$) in the ring current are investigated based on ion composition measurements (<180 keV/q) by medium-energy particle experiments-electron analyzer and low-energy particle experiments-ion mass analyzer instruments on board the Arase (Exploration of energization and Radiation in Geospace, ERG) satellite. The investigated period from late March to December 2017 includes 11 geomagnetic storms with the minimum Dst index less than −40 nT. The molecular ions are observed in the region of L = 2.5–6.6 and clearly identified at energies above ~12 keV during most magnetic storms. During quiet times, molecular ions are not observed. The average energy density ratio of the molecular ions to O^+ is ~3%. The ratio tends to increase with the size of magnetic storms. Existence of molecular ions even during small magnetic storms suggests that the fast ion outflow from the deep ionosphere occurs frequently during geomagnetically active periods.

Plain Language Summary Molecular ions usually exist only in the low-altitude (< 300 km) deep ionosphere and cannot escape to space without a fast ion outflow to overcome a rapid loss due to dissociative recombination. Thus, molecular ion escape from the terrestrial atmosphere to space can be used as a tracer of effective ion loss from the deep ionosphere. Here we report new observations by Arase satellite that enables definitive identification of molecular ions by frequent time-of-flight mode observations. The statistical analysis shows that molecular ions exist in near-Earth space during most magnetic storms, while they are not detected during geomagnetically quiet periods. The existence of molecular ions even during small magnetic storms suggests that the magnetic storm is an effective driver of the ion loss from the deep terrestrial ionosphere.

1. Introduction

There have been reports on molecular ion observations in the magnetosphere (e.g., Christon et al., 1994; Craven et al., 1985; Klecker et al., 1986; Lennartsson et al., 2000) and in the high-altitude ionosphere (e.g., Peterson et al., 1994; Wilson & Craven, 1999; Yau et al., 1993) under extreme geomagnetic conditions such as during large magnetic storms. Klecker et al. (1986) discovered energetic (>80 keV/q) molecular ions (NO^+/O_2^+) in the storm-time ring current by AMPTE/IRM and showed that the molecular ion flux with 160 keV/q at L = 7–9 is a few percent of O^+. They also pointed out that the molecular ions are below the detection limit during quiet (Kp < 3) periods. Christon et al. (1994) reported high-energy molecular ions ($N_2^+/NO^+/O_2^+$) in the plasma sheet in the distant magnetotail at X_{GSM} = −146 R_E at energies above 80 keV/e also during an extremely active period of $Kp = 7^-$. There is also a report of possible molecular ion detection at the lunar orbit by THEMIS (Time History of Events and Macroscale Interactions during Substorms) (Poppe et al., 2016). However, since the instrument has no mass discrimination, it is likely that the ion beam mainly consists of O^+ rather than molecular ions (private communication).

The existence of molecular ions in the magnetosphere is not explicable with the ordinary ion outflow mechanisms from the terrestrial ionosphere (e.g., André & Yau, 1997; and references therein). While the ion upflows usually start at the altitude above 400 km (Foster et al., 1998; Ogawa et al., 2008), the empirical model of the terrestrial ionosphere indicates that molecular ions exist only in the low-altitude ionosphere below 300 km altitude (e.g., Bilitza & Reinisch, 2008). In order for the molecular ions to outflow to the

magnetosphere, they need to acquire the escape energy within a short time scale compared with the local dissociative recombination lifetime of the molecular ions. The time scale is a few minutes around 300 km altitude. Thus, the molecular ions can be a tracer of the fast ion outflow from the low-altitude deep ionosphere (< 300-km altitude).

Peterson et al. (1994) reported low-energy (> 15 eV) molecular ions ($O_2^+/NO^+/N_2^+$) in polar regions at altitudes of 5,000–10,000 km observed by Akebono during three geomagnetically active periods (one event with $Kp{\sim}9^-$ and two events with $Kp{\sim}3^+$). They assessed possible candidate mechanisms to cause the fast molecular ion outflow and concluded that neither Joule heating, ion resonance heating, nor large-scale field-aligned current instabilities are strong enough to achieve the molecular ion outflows. They also suggested that a remaining candidate may be localized acceleration and/or heating due to intense high-frequency lower-hybrid plasma waves. In addition to their argument, there is a possibility of localized convection enhancement such as subauroral ion drifts (Anderson et al., 1991) and subauroral polarization streams (Foster & Vo, 2002), and the resultant Joule heating during the magnetic storms can cause the localized molecular ion outflows (Wilson & Craven, 1999; Zettergren et al., 2011).

As described above, reports on molecular ion observations in the ring current are limited to some event studies (e.g., Klecker et al., 1986) and their statistical properties are far from understood. In this study, we report on the statistical properties of the molecular ions observed by the Arase (ERG: Exploration of energization and Radiation in Geospace) satellite utilizing abundant time-of-flight (TOF) mode observations enabling us a definitive identification of molecular ions. In section 2, the data set used and identification method of molecular ions are explained. We then show the statistical properties of molecular ions in section 3, which is followed by discussions in section 4 and conclusion in section 5.

2. Data Analysis and Identification Methods of Molecular Ions

2.1. Data Set

The Arase (ERG) satellite was launched in December 2016 and started its science operation from late March in 2017 aiming at understanding of dynamic variation in geospace with a focus of acceleration and loss mechanisms of the relativistic electrons in the radiation belts (Miyoshi et al., 2018). The apogee, perigee, and inclination of Arase are ~32,000, ~400 km, and 31°, respectively. In this study, we use data from four instruments on board Arase: Medium-energy particle experiments-electron analyzer (MEPe, Kasahara et al., 2018) and ion mass analyzer (MEPi, Yokota et al., 2017), low-energy particle experiments-ion mass analyzer (LEPi, Asamura et al., 2018), and extremely high energy electron experiment (XEP, Higashio et al., 2018). The energy range of LEPi, MEPe, and XEP instruments are 0.01–25 keV/q, 7–87 keV, and 0.4–20 MeV, respectively. The spin period of the Arase satellite is ~8 s. Since the TOF mode observations of LEPi are less frequent than those of MEPi, we mainly use the MEPi data for this statistical study of molecular ions. LEPi data are used to check the consistency of molecular ion identification at low energies, when the TOF data are available. McIlwain's L parameter with International Geomagnetic Reference Field: the 11th generation is used to infer the distance where the local magnetic flux tube at the Arase satellite crosses the equatorial plane.

In order to conduct a statistical survey, we use the Arase data from 26 March to 31 December 2017, which corresponds to the declining phase of the Solar Cycle 24. Note that LEPi started the regular operation since April 2017. Since there was an operation of the high voltage change of MEPi in early 2018 and the absolute data calibration for data after the operation is still ongoing, we decided to use the data only in 2017 for this study. For definitive identification of molecular ions, we used TOF data from MEPi and LEPi instruments, in which we can examine the count distribution of each ion species. The TOF data usually have time resolution of 16 s. It should be noted that both MEPi and LEPi do not have enough mass resolution to distinguish between O^+ and N^+ as well as between O_2^+, NO^+, and N_2^+. In the labels of some figures and the related text, we use O^+ (O_2^+, NO^+) to represent the N^+/O^+ group ($O_2^+/NO^+/N_2^+$ group). However, it does not exclude contribution of N_2^+ to molecular ions, since N_2^+ are sometimes comparable to NO^+ in the source ionospheric upflows (Yau et al., 1993).

The ion count data from MEPi are accumulated over 30 min in this study, in order to conduct O^+ contamination (noise) reduction described in section 2.2. The MEPi TOF data at each time interval consist of 4

azimuthal angles, 15 energy channels, and 512 TOF bins. Before 23 April 2017, the MEPi energy range used for the molecular ion identification was 8 to 110 keV/q, and it was raised from 10 to 185 keV/q after the date. The ring current (MEPe) and radiation belt (XEP) electron data are used to be compared with ring current ions and the noise level derived from the MEPi data, respectively.

2.2. Identification of Molecular Ions

In this subsection, we explain the data analysis method to remove false detection of molecular ions and derive precise energy density ratio of molecular ions against O^+ by subtracting the O^+ contamination to the molecular ion TOF bins. Figure 1 shows an example event of molecular ion observations during a weak magnetic storm with the minimum Dst of −44 nT. Before the start of the main phase (time interval shown by the left-hand magenta box in Figure 1), Arase observed the H^+ dominant ring current and well-developed electron radiation belts. During this period, both MEPi and LEPi instruments detected significant counts in the molecular ion TOF range. The counts become larger with decreasing energy as shown in Figure 1. On the other hand, during the main and recovery phases, molecular ion counts are also detected (sixth panel from the top), but they are more structured in energy and similar to that of O^+ (fifth panel). These data indicate that simple identification of molecular ions with determined TOF bins can include false counts due to contamination from O^+ and/or noise due to high-energy electrons.

Therefore, we here introduce a fitting method to eliminate the noise counts from molecular ion count data. In order to eliminate noise counts both from O^+ and high-energy electrons we use linear combination of a Gaussian and a baseline as the fitting function:

$$f(x) = A_0 e^{-\frac{1}{2}\left(\frac{x-A_1}{A_2}\right)^2} + A_3 + A_4 x$$

After checking many TOF distributions in both quiet and disturbed periods, we adopted this fitting function, which can be adjusted to various cases of background counts. Figure 2 shows two examples of the application of the fitting. Figures 2a and 2b correspond to the two intervals (before the main phase and around the storm peak: minimum Dst) shown by magenta boxes in Figure 1.

First, we fit the above function to the count data in the TOF range shown with magenta symbols in each panel. Note that the TOF bins used for the fitting (magenta symbols) start from the minimum TOF bin assigned for O^+ ions (yellow shade) and exclude the TOF range for molecular ions (gray shade), but including the same number of bins as the molecular ion range above it. In order to assure the quality of the fitting, we applied the fitting only to the data with original O^+ counts ≥200 and molecular ion counts ≥10 at each energy channel. The resultant fitting function shown by a red curve is utilized to calculate the noise counts at each TOF bin. Then the noise counts are subtracted from the original data, and we get the molecular ion counts in the TOF range assigned for them shown by blue symbols in Figure 2. The procedure is conducted for data at each energy channel. Then the corrected counts are used for moment calculations of molecular ions. The energy density threshold with this identification method depends on the characteristic energy of molecular ions and the noise level due to the relativistic electrons. The resultant molecular ion energy density ranges mostly above 10^{-3} (keV/cm^3).

As shown in Figure 2, the corrected counts (blue symbols) before the storm main phase (Figure 2a) are less than the noise level (red curve) in the molecular ion range (gray shade). It indicates that the observed counts in the molecular ion range in this time interval are mainly the noise counts. On the other hand, during the main phase (Figure 2b), the corrected counts have a significant peak in the molecular ion TOF range and the peak is well above the noise level. Thus, we can conclude that the molecular ions are definitively detected during the period. For definitive identification of molecular ions, we calculate the ratio of the peak corrected counts against the noise level at each energy as shown in the fourth panel from the bottom in Figure 1, and we regarded that the data with the peak noise ratio above 2 as a clear observation of the molecular ions. During the interval shown in Figure 1, the result indicates that molecular ions are observed during the main and recovery phases of the weak storm but not before the storm main phase.

We then calculate the energy density ratio between molecular ions ($O_2^+/NO^+/N_2^+$) and O^+ using data that satisfy the above identification criteria. As shown in the third panel from the bottom in Figure 1, the energy

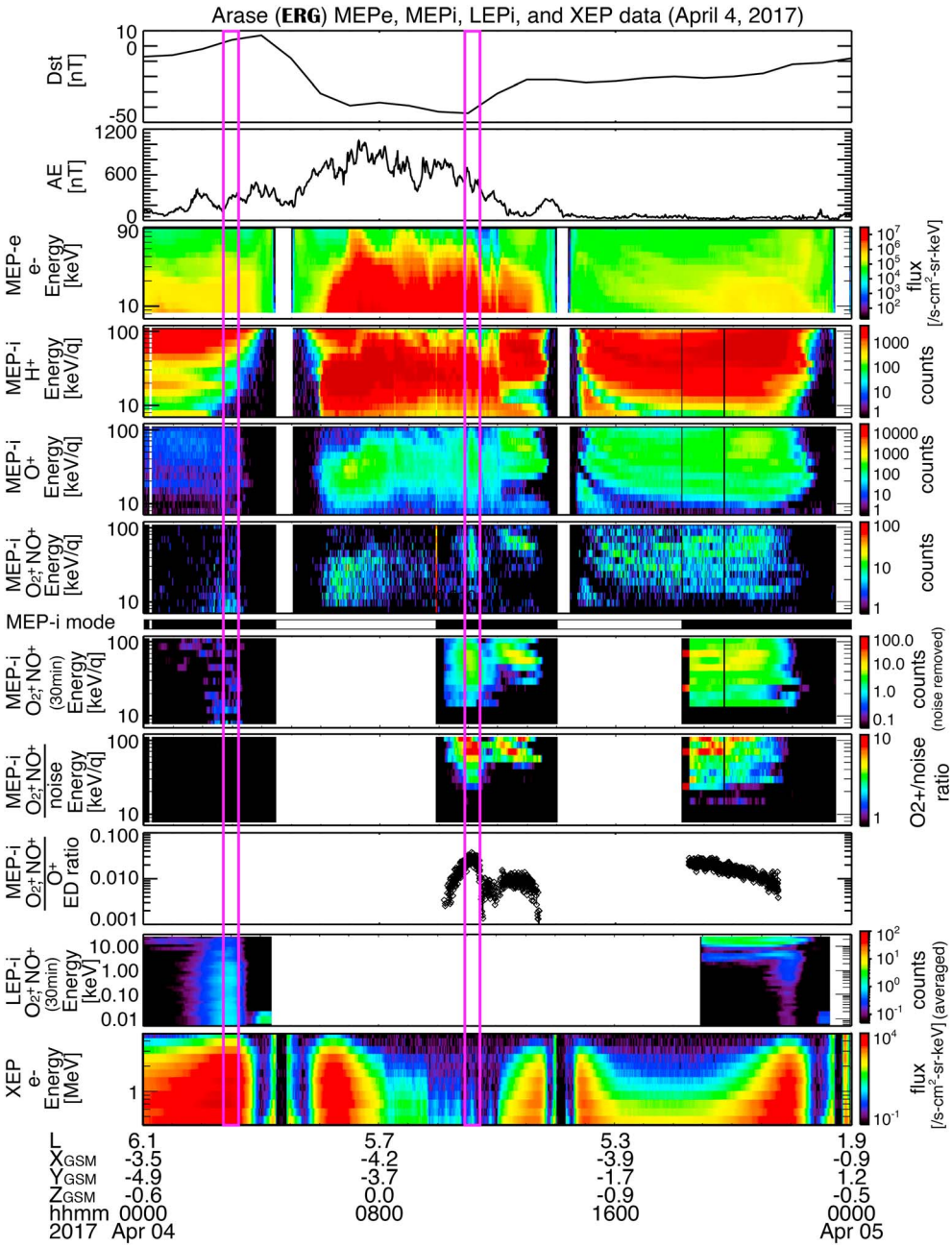

Figure 1. Summary plots to show Arase (ERG) observations on 4 April 2017, which includes geomagnetic disturbance with minimum Dst of −44 nT. The top six panels of the figure show Dst and AE indices, omnidirectional energy-time spectrograms of electrons, H^+, O^+, and molecular ions, respectively. The black bars below the six panels indicate time intervals when the MEPi instrument on board Arase was operated in the TOF (time-of-flight) mode. Below the bars, molecular ion counts averaged over 30 min with O^+ contamination (noise) reduction described in the text, ratio of molecular ion counts against the noise counts at each energy, and energy density ratio of molecular ions to O^+ are shown. The bottom two panels show energy-time spectrograms for the 30-min averaged counts of molecular ions for low- energy ions from LEPi and relativistic electron counts from XEP, respectively. Magenta boxes correspond to the time intervals used to plot the TOF data shown in Figure 2. MEPi = Medium-energy particle experiments-ion mass analyzer; LEPi = low-energy particle experiments-ion mass analyzer; XEP = extremely high energy electron experiment; MEPe = medium-energy particle experiments-electron analyzer.

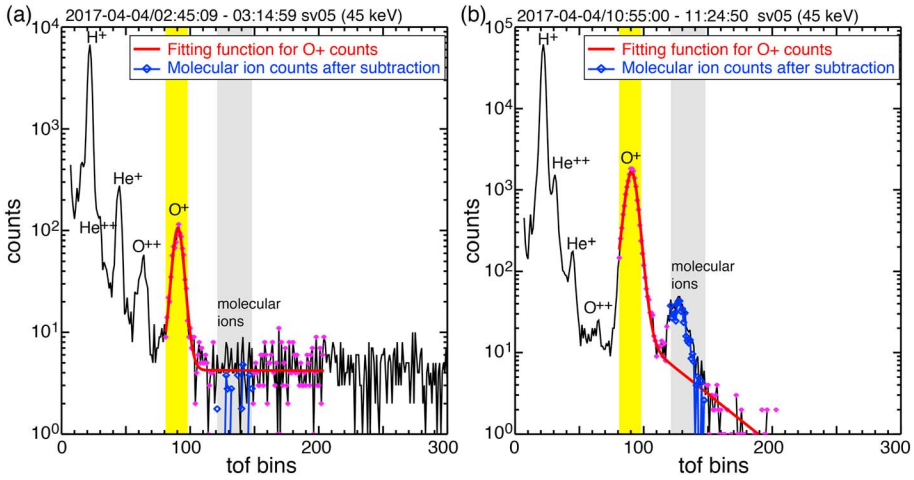

Figure 2. Examples of O^+ contamination reduction from molecular ions ($O_2^+/NO^+/N_2^+$) with a fitting method described in the text. Raw TOF (time-of-flight) count data obtained by MEPi instrument for the energy bin of ~45 keV are shown in black lines as a function of TOF bins for two 30-min intervals shown by magenta boxes in Figure 1: (a) initial phase and (b) around Dst minimum of the small geomagnetic storm. Each peak of the TOF data is labeled with corresponding ion species. The red lines and magenta symbols show the fitting function for O^+ counts and the TOF range used for the fitting, respectively. Blue symbols with line indicate molecular ion counts after subtraction of O^+ contamination using the fitting function. The yellow and gray shaded areas correspond to the TOF ranges used for moment calculations of O^+ and molecular ions, respectively. MEPi = medium-energy particle experiments-ion mass analyzer.

density ratio of molecular ions (represented by O_2^+, NO^+) to O^+ is in the order of 1% during this time interval. We also verified that the energy range of molecular ions is consistent with that of LEPi observations. We applied these methods to investigate statistical properties of molecular ions in the ring current for the time period from 26 March to 31 December 2017.

3. Statistical Properties of Molecular Ions in the Ring Current

During the time period from late March to December 2017 used in this statistical study of molecular ions in the ring current, there occurred 11 geomagnetic storms with a minimum Dst index less than −40 nT as shown in the top panel of Figure 3. Coinciding with the storms, the Arase satellite observed development of both electron and ion ring currents at $L = 5$ as shown in the fourth to ninth panels in Figure 3. Comparison between H^+ and O^+ ions show that energy of the ring current ions tends to be higher for H^+ than O^+. Relativistic electrons in the outer radiation belt at $L = 5$ also shows variation coinciding with the geomagnetic variations (third panel from the top). When the relativistic electron flux is high, we see some noise counts in the raw O_2^+/NO^+ data (second panel from the bottom). As shown in the third panel from the bottom of Figure 3, the noise is eliminated after the noise reduction explained in section 2.2 in the corrected O_2^+/NO^+ data.

The time intervals when molecular ions are clearly identified can be seen in the bottom panel of Figure 3, which shows the energy density ratio of O_2^+/NO^+ to O^+. In the panel, green color indicates molecular ion observations at all L values, while black shows observations at $L = 5$. As shown, the molecular ions are observed during most of the geomagnetic storms as well as some geomagnetic disturbances with Dst ~ −30 nT. The molecular ions are clearly identified at energies above ~14 keV and the O_2^+/NO^+ to O^+ energy density ratio ranges from 0.1% to 10%. It should be noted that we did not observe the molecular ions during the geomagnetic disturbance in December 2017. It is partially because of degradation in the MEPi sensitivity over time. We observed some weak peaks of molecular ion counts in TOF data on 5 December 2017 during a magnetic storm, but they were below the identification threshold of the molecular ions used in this study (not shown).

As shown in Figure 4a, molecular ions are observed over a wide range of the local times from dawn to dusk. They are observed mainly in the region of $L = 3.5$–6.6 (Figure 4b). Their detection probability becomes higher for larger magnetic storms (Figure 4c) as well as during substorms (Figure 4d). The energy density

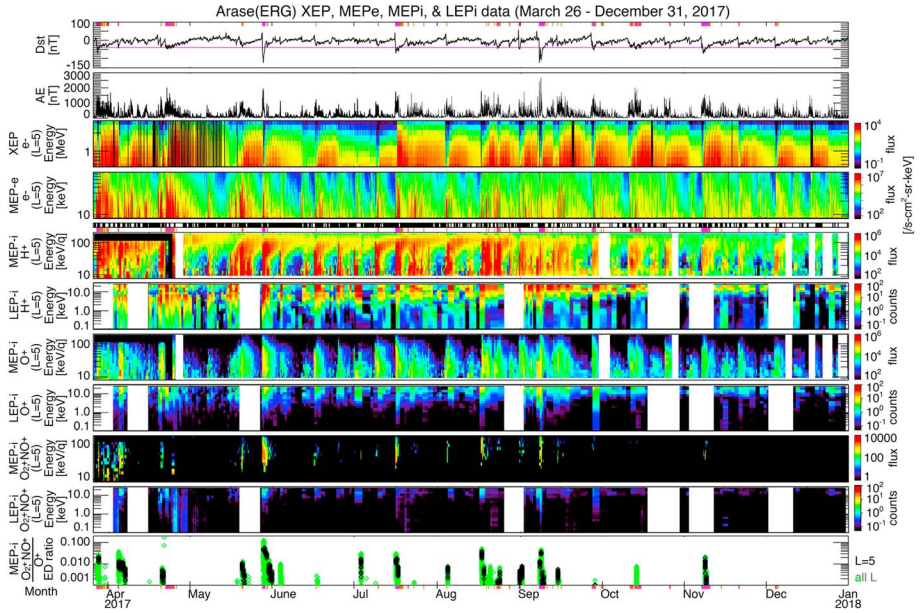

Figure 3. Summary plots of molecular ion observations in the ring current for the interval from 26 March to 31 December 2017. The top four panels show the Dst (with horizontal magenta line showing -40 nT) and AE indices, omnidirectional energy-time spectrograms for relativistic electrons observed at $L = 5$ by XEP, and middle-energy electrons from MEPe, respectively. The black bars below these panels indicate time intervals when MEPi was operated in the TOF mode. The color bars at the top, below the TOF bars, and at the bottom of the figure display time intervals when Dst ranges between −30 and −40 nT (orange) and below −40 nT (magenta). Below the middle color bars, omnidirectional energy-time spectrograms observed by MEPi and LEPi for H^+, O^+, and molecular ions (represented by O_2^+, NO^+) are shown. The bottom panel displays the energy density ratio of the O_2^+/NO^+ to O^+ for the time periods when molecular ion counts are clearly detected, with green symbols for all L values and black for $L = 5$. MEPi = Medium-energy particle experiments-ion mass analyzer; LEPi = low-energy particle experiments-ion mass analyzer; XEP = extremely high energy electron experiment; MEPe = medium-energy particle experiments-electron analyzer.

ratio of O_2^+, NO^+ to O^+ also tends to be higher for larger storms. As for the energy density of molecular ions, there are four geomagnetically disturbed periods in which the O_2^+, NO^+ energy density exceeds 1 keV/cm^{-3}. The peak energy density of each event is observed on 28 May, 16 July, 17 August, and 8 September 2017, respectively. The maximum O^+ (O_2^+/NO^+) energy densities observed around minimum Dst during the four events are 172 (5.3), 133 (3.2), 34 (1.7), and 220 (3.5), respectively. Among the four high-energy density events, energy density of O^+ ions are at a high level on 28 May, 16 July, and 8 September 2017, while during 17 August event, only molecular ions are at high-energy density level compared to other events. Note that exceptionally high O_2^+, NO^+ to O^+ energy density ratio of 0.13 was observed in the 28 May event, when the Arase satellite was located at high L~6.6 where the O^+ energy density is lower than the main part of the ring current (L~3.7).

We investigated dependences on various solar wind parameters such as the solar wind dynamic pressure, density, velocity, convection electric field, and interplanetary magnetic field (IMF) orientation and strength. The molecular ions in the ring current tend to be observed during the high dynamic pressure periods. The dependence is mostly resultant from the solar wind velocity. While there is no clear dependence of molecular ion detection probability on the solar wind density (Figure 4e), the dependence on the solar wind velocity (Figure 4f) stands out the most among the solar wind parameters. The dependence on the solar wind velocity is clearer than that on the dynamic pressure.

4. Discussions

As introduced in section 1, previous studies of the molecular ion observations in the Earth's ring current are limited to a few event studies. Most of the molecular ion observations in the magnetosphere or high-altitude ionosphere (e.g., Christon et al., 1994; Klecker et al., 1986; Peterson et al., 1994; Yau et al., 1993) were made

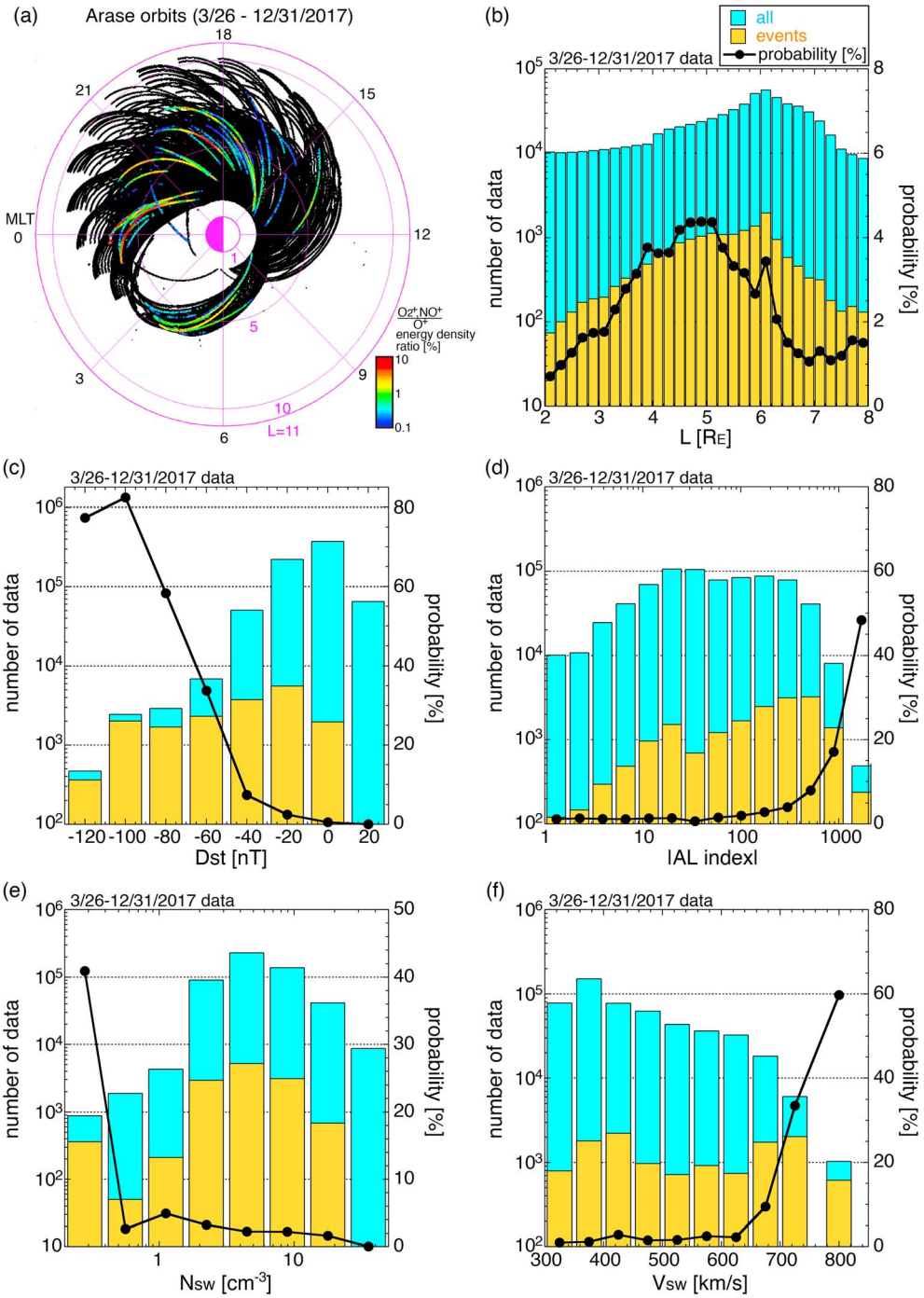

Figure 4. Spatial distribution and statistical dependences on geomagnetic indices and solar wind parameters of molecular ions in the ring current. (a) Black lines show the Arase orbital coverage on the magnetic equatorial plane with MEPi TOF observations, where radial distance from the center indicates the McIlwain's *L* parameter (magenta labels) and angle displays the MLT (magnetic local time, black labels). Distribution of color points shows the location of the clear molecular ion identification, and the color code corresponds to molecular (O_2^+, NO^+) to O^+ energy density ratio. (b–f) Histograms of all Arase data used (light blue bars) and molecular ion detection (orange bars) against the (b) *L* parameter, (c) Dst index, (d) absolute value of AE index, (e) solar wind density, and (f) solar wind velocity are shown, respectively, together with the occurrence frequency of molecular ion detection at each parameter range (black circles and lines).MEPi = Medium-energy particle experiments-ion mass analyzer; TOF = time of flight.

under active geomagnetic conditions ($Kp > 3^+$). When we check the Kp index during the present observations for comparison, molecular ions are detected even during moderate geomagnetic conditions as low as $Kp = 2^-$. The average observational probability of the molecular ions in the ring current is about 2.4% including quiet periods, and the probability is higher than that at high-latitude regions (<1%) reported by Lennartsson et al. (2000). The probability increases drastically with increasing geomagnetic activities (Figures 4c and 4d). These results indicate that the existence of molecular ions in the ring current is a common phenomenon during geomagnetically disturbed periods and that extreme geomagnetic conditions are not necessary. The average molecular ($O_2^+/NO^+/N_2^+$) to O^+ ion energy density ratio is about 1.4 % for the surveyed period from 26 March to 31 December 2017. As shown in Figure 3, it can exceed 5% during large magnetic storms. The ratio is in the same order of the ion flux ratio of a few percent at 160 keV/q reported by Klecker et al. (1986).

During the period, there are four magnetic storms in which the high-energy density of molecular ions is pronounced. Among the four events, three of them correspond to CME-driven magnetic storms. During the CME (coronal mass ejection)-driven events, the O^+ energy density is also increased more than usual. It might be related to the stronger upflow flux in the ionosphere during CME-driven storms than those in CIR (corotating interaction region)-driven storms observed by European Incoherent Scatter (EISCAT) radar (Ogawa et al., 2019). However, the molecular ion event on 17 August is detected during a CIR-driven magnetic disturbance and the geomagnetic conditions measured with Dst are more moderate (Dst ~−20 nT) than during the other three events. During this CIR event, O^+ energy density did not increase significantly. Together with the observed correlation between molecular ions detection probability and the solar wind velocity as well as the AL index, it is suggested that the cause of relatively high molecular ion energy density results from multiple conditions.

5. Summary and Conclusion

Utilizing frequent TOF-mode observations by Arase/MEPi, we investigated statistical properties of molecular ions ($O_2^+/NO^+/N_2^+$) in the ring current of the Earth's magnetosphere during the period from 26 March to 31 December 2017. Results show as follows.

1. The molecular ions are observed in association with geomagnetic disturbances with Dst < −30 nT. During quiet times, molecular ions are not observed. The tendency is consistent with previous observations.
2. The molecular ions are observed mainly in the region of L = 3.5–6.6 and clearly identified at energies above ~14 keV with molecular to O^+ ion energy density ratio of the order of 1%.
3. Detection probability of molecular ions in the ring current becomes higher with increasing size of geomagnetic storms (minimum Dst index).
4. Their detection probability also tends to be higher during substorms as well as during high-speed solar wind period.

The observations reveal that existence of molecular ions in the ring current is a frequent phenomenon during geomagnetically moderate and active periods. The fact might indicate that the rapid transport/heating in the low-altitude ionosphere to cause molecular ion outflows is rather common during moderate geomagnetic disturbances. The observation probability of the molecular ions in the ring current is comparable or higher than that in the high-altitude auroral regions, suggesting the importance of the subauroral zone. In order to understand the outflow mechanism, simultaneous observations of ion upflows in the low-altitude ionosphere by EISCAT radars will be useful.

Acknowledgments
This work is supported by MEXT/JSPS KAKENHI grants JP16H06286 (Grant-in-Aid for Specially Promoted Research), JP16H02229 (Grant-in-Aid for Scientific Research (A)), JP17K14400 (Grant-in-Aid for Young Scientists (B)), JP15H05815 (Grant-in-Aid for Scientific Research on Innovative Areas), and JP15H05747 (Grant-in-Aid for Scientific Research (S)). Science data of the ERG (Arase) satellite were obtained from the ERG Science Center (ERG-SC) operated by ISAS/JAXA and ISEE/Nagoya University (https://ergsc.isee.nagoya-u.ac.jp/index.shtml.en). The Arase satellite data become publicly available via ERG-SC on a project-agreed schedule. The present study analyzed the LEPi TOF L1-v01, MEPi NML L2-v01 03 and TOF L2-v01_00, MEPe L2-v01_01, and XEP L2-v00_00 data obtained by Arase. The data management of XEP/Arase was supported by the JAXA/SEES. The Arase orbital data L2-v02 is also used. The Dst, AL, and AE indices were obtained from the World Data Center for Geomagnetism, Kyoto, Kyoto University (http://wdc.kugi.kyoto-u.ac.jp/index.html). The solar wind data are extracted from NASA/GSFC's OMNI data set through OMNIWeb (https://omniweb.sci.gsfc.nasa.gov). Part of the work of T. H., M. T., and Y. M. was done at ERG-SC.

References

Anderson, P. C., Heelis, R. A., & Hanson, W. B. (1991). The ionospheric signatures of rapid subauroral ion drifts. *Journal of Geophysical Research*, *96*(A4), 5785–5792. https://doi.org/10.1029/90JA02651

André, M., & Yau, A. (1997). Theories and observations of ion energization and outflow in the high latitude magnetosphere. *Space Science Reviews*, *80*(1–2), 27–48.

Asamura, K., Kazama, Y., Yokota, S., Kasahara, S., & Miyoshi, Y. (2018). Low-energy particle experiments-ion mass analyzer (LEPi) onboard the ERG (Arase) satellite. *Earth, Planets and Space*, *70*(1). https://doi.org/10.1186/s40623-018-0846-0

Bilitza, D., & Reinisch, B. W. (2008). International reference ionosphere 2007: Improvements and new parameters. *Advances in Space Research*, *42*(4), 599–609. https://doi.org/10.1016/j.asr.2007.07.048

Christon, S. P., Gloeckler, G., Williams, D. J., Mukai, T., McEntire, R. W., Jacquey, C., et al. (1994). Energetic atomic and molecular ions of ionospheric origin observed in distant magnetotail flow-reversal events. *Geophysical Research Letters*, *21*(25), 3023–3026. https://doi.org/10.1029/94GL02095

Craven, P. D., Olsen, R. C., Chappell, C. R., & Kakani, L. (1985). Observations of molecular ions in the Earth's magnetosphere. *Journal of Geophysical Research*, *90*(A8), 7599–7605. https://doi.org/10.1029/JA090iA08p07599

Foster, C., Lester, M. T., & Davies, J. A. (1998). A statistical study of diurnal, seasonal and solar cycle variations of *F*-region and topside auroral upflows observed by EISCAT between 1984 and 1996. *Annales de Geophysique*, *16*(10), 1144–1158. https://doi.org/10.1007/s00585-998-1144-0

Foster, J. C., & Vo, H. B. (2002). Average characteristics and activity dependence of the subauroral polarization stream. *Journal of Geophysical Research*, *107*(A12), 1475. https://doi.org/10.1029/2002JA009409

Higashio, N., Takashima, T., Shinohara, I., & Matsumoto, H. (2018). The extremely high-energy electron experiment (XEP) onboard the Arase (ERG) satellite. *Earth, Planets and Space*, *70*(1). https://doi.org/10.1186/s40623-018-0901-x

Kasahara, S., Yokota, S., Mitani, T., Asamura, K., Hirahara, M., Shibano, Y., & Takashima, T. (2018). Medium-energy particle experiment-electron analyzer (MEP-e) for the exploration of energization and radiation in geospace (ERG) mission. *Earth, Planets and Space*, *70*(1). https://doi.org/10.1186/s40623-018-0847-z

Klecker, B., Möbius, E., Hovestadt, D., Scholer, M., Gloeckler, G., & Ipavich, F. M. (1986). Discovery of energetic molecular ions (NO^+ and O_2^+) in the storm time ring current. *Geophysical Research Letters*, *13*(7), 632–635. https://doi.org/10.1029/GL013i007p00632

Lennartsson, O. W., Collin, H. L., Peterson, W. K., & Shelley, E. G. (2000). Polar/TIMAS statistical results on the outflow of molecular ions from earth at solar minimum. *Advances in Space Research*, *25*(12), 2417–2420. https://doi.org/10.1016/S0273-1177(99)00531-1

Miyoshi, Y., Shinohara, I., Takashima, T., Asamura, K., Higashio, N., Mitani, T., et al. (2018). Geospace exploration project ERG. *Earth, Planets and Space*, *70*(1). https://doi.org/10.1186/s40623-018-0862-0

Ogawa, Y., Seki, K., Hirahara, M., Asamura, K., Sakanoi, T., Buchert, S. C., et al. (2008). Coordinated EISCAT Svalbard radar and Reimei satellite observations of ion upflows and suprathermal ions. *Journal of Geophysical Research*, *113*, A05306. https://doi.org/10.1029/2007JA012791

Ogawa, Y., Seki, K., Keika, K., & Ebihara, Y. (2019). Characteristics of CME- and CIR-driven ion upflows in the polar ionosphere. *Journal of Geophysical Research: Space Physics*, *124*, 3637–3649. https://doi.org/10.1029/2018JA025870

Peterson, W. K., Abe, T., Fukunishi, H., Greffen, M. J., Hayakawa, H., Kasahara, Y., et al. (1994). On the sources of energization of molecular ions at ionospheric altitudes. *Journal of Geophysical Research*, *99*(A12), 23,257–23,274. https://doi.org/10.1029/94JA01738

Poppe, A. R., Fillingim, M. O., Halekas, J. S., Raeder, J., & Angelopoulos, V. (2016). ARTEMIS observations of terrestrial ionospheric molecular ion outflow at the Moon. *Geophysical Research Letters*, *43*, 6749–6758. https://doi.org/10.1002/2016GL069715

Wilson, G. R., & Craven, P. (1999). Molecular ion upflow in the cleft ion fountain. *Journal of Geophysical Research*, *104*(A3), 4437–4446. https://doi.org/10.1029/1998JA900070

Yau, A. W., Whalen, B. A., Goodenough, C., Sagawa, E., & Mukai, T. (1993). EXOS-D (AKEBONO) observations of molecular NO^+ and N_2^+ upflowing ions in the high-altitude auroral ionosphere. *Journal of Geophysical Research*, *98*(A7), 11,205–11,224. https://doi.org/10.1029/92JA02019

Yokota, S., Kasahara, S., Mitani, T., Asamura, K., Hirahara, M., Takashima, T., et al. (2017). Medium-energy particle experiments-ion mass analyzer (MEP-i) onboard ERG (Arase). *Earth, Planets and Space*, *69*(1). https://doi.org/10.1186/s40623-017-0754-8

Zettergren, M., Semeter, J., Heinselman, C., & Diaz, M. (2011). Incoherent scatter radar estimation of *F* region ionospheric composition during frictional heating events. *Journal of Geophysical Research*, *116*, A01318. https://doi.org/10.1029/2010JA016035